POINT BASED REGISTRATION OF TERRESTRIAL LASER DATA USING INTENSITY AND GEOMETRY FEATURES

Zhi Wang [a,b,] * and Claus Brenner [a]

[a] Institute of Cartography and Geoinformatics, Leibniz Universität Hannover,
Appelstraße 9a, D-30167 Hannover, Germany
-wangzchina@gmail.com, - Claus.Brenner@ikg.uni-hannover.de
[b] State Key Laboratory for Information Engineering in Surveying, Mapping and Remote Sensing,
Wuhan University, Luoyu Road, Wuhan, China, 430079

Commission V/3 - Terrestrial Laser Scanning

KEY WORDS: Laser scanning, Registration, Algorithms, Point cloud, TLS, Geometry

ABSTRACT:

Terrestrial laser scanning provides a three-dimensional sampled representation of the surfaces of terrestrial objects. The fully automatic registration of terrestrial laser scanning point-clouds is still a question as it involves handling huge datasets, irregular point distribution, multiple views, and relatively low textured surfaces. In this paper, we propose a key point based method using intensity and geometry features for the automatic marker-free registration of terrestrial laser scans. We apply the SIFT method for extracting feature points from the reflectance image and geometric constraint for excluding false matches. To evaluate the performance of proposed method, we employ a test scene in downtown Hannover, Germany. Reference orientations were acquired by the standard orientation procedure using retro-reflective targets and manually assisted target selection. In the experiments, we present the results of the proposed method regarding performance, accuracy and running time for the test scene.

1. INTRODUCTION

Terrestrial laser scanning provides a three-dimensional sampled representation of the surfaces of terrestrial objects, such as buildings, sculptures and so on. In most cases, the acquisition of several scans is needed to obtain full scene coverage, and therefore the data collected from different locations of a scanner must be transformed into one global reference frame. The fully automatic registration of terrestrial laser scanning point-clouds is still a question as it involves handling huge datasets, irregular point distribution, multiple views, and relatively low textured surfaces. If a good priori alignment is provided and the point clouds share a large overlapping region, existing registration methods, such as the Iterative Closest Point (ICP, (Besl and McKay, 1992)) or Chen and Medioni's method (Chen and Medioni, 1991), work well (for a comparison, see (Rusinkiewicz and Levoy, 2001)). However, in practical applications of laser scanners, partially overlapping and unorganized point clouds are usually provided without good initial alignment. In these cases, the existing registration methods are not appropriate since it becomes very difficult to find the correspondence of the point clouds.

2. CURRENT APPROACHES AND OPEN QUESTIONS

For practical purposes, the identification of tie points between scans is nowadays solved using artificial markers which are set up in the scene prior to scanning. Using retro-reflective materials, they can be detected automatically in the laser scan using threshold methods. However, distribution and collection of the targets is quite time-consuming and often exceeds the net scanning time by a factor of five (Brenner et al., 2008). Furthermore, due to practical requirements, an optimal distribution often cannot be obtained, resulting in a non-optimal distribution of registration errors. In those cases, it would be desirable to select tie points evenly distributed in the overlapping scan volume.

To addresses the above problems, there has been extensive research for developing automatic registration of terrestrial laser scans. Brenner et al. (2008) investigate two different registration methods targeted at the determination of suitable initial values. The first one is based on planar patches, using corresponding planar features to compute the orientation. In their autonomous method, following the extraction of planar patches from different scans, plane triples are assigned, transformations are computed and scored, and the transformation with the highest score wins. However, the extraction and assignment of the planar patches may become a quite complex task in the case of confusional scenes. The second one is a non-symbolic approach based on an iterative alignment scheme using the normal distributions transform. Barnea and Filin (Barnea and Filin, 2008) present a computational approach for the registration problem. They exploit 3D rigid-body transformation invariant features to reduce significantly the computational load involved in the matching between key features. Bae and Lichti (Bae and Lichti, 2004) use variation in geometric curvature and approximate normal vector of the surface to determine the possible correspondence of point clouds. This requires the computation of the normal vector and the curvature itself. These descriptors have high potential to be effected by noise because of the dependency on second-order derivatives.

Recently, there have been approaches to extract tie points in laser scans without artificial markers using the well-known scale invariant feature transform (SIFT, (Lowe, 2003)). This

method has originally been developed for image matching and has been shown to be robust against changes in illumination, scale, rotation and affine distortion. Since most terrestrial laser scanners have the ability to capture images as well, the obvious way to use SIFT for laser scans is to extract feature points from the images first, and then compute their 3D coordinates using the known relative orientation of camera and scanner (Bendels et al., 2004; Barnea and Filin, 2008). However, Böhm and Becker (2007) have even shown that good results can be obtained by applying the SIFT operator to the reflectance image of the scanner directly.

Inspired by this, it has been our goal to improve these results.We address the major drawbacks of the methods which use SIFT features directly. First, SIFT has been deliberately built to work across huge scale and viewpoint differences. However, using laser scans, the scale and viewpoint are known. Second, applying SIFT in the image or reflectance data only ignores the geometric information available in the scan data. Therefore, geometric important features may be ignored by SIFT method if they are not so distinctive in the reflectance image. On the other hand, SIFT will be indifferent to high responses that are due to the actual features, or to fake ones resulting from objects partially covering an object in the background and thus creating a feature-like effect. The latter may lead to false matches. Thus, it was our goal to improve the extraction of interest points by incorporating geometric information.

In this paper we present an automatic registration method, using geometric feature-point matching. Geometric curvature (e.g., the Gaussian and mean curvature) is invariant to 3D rigid motion. Therefore, the change of geometric curvature of the surface formed by a point and its neighborhood are used for selecting the possible correspondences of point clouds. We add the Gaussian, mean curvature values to the SIFT feature descriptor vector so that not only the gray values but the surface geometric properties take part in the detecting and matching of feature-points to optimize the matching process and reduce the computational cost involved in the matching between geometric features. We also show how the information embedded within the range data is utilized to improve the quality of the selected geometric feature points, such as discarding the fake features (resulting from partially occluded objects) by distinguishing layered surfaces with respect to their distances.

2.1 Registration methods

Registration of terrestrial laser scanning data is to find the rotation and translation parameters which makes corresponding locations in the two point clouds SP_1 and SP_2 coincide. Due to the six degrees of freedom to place and orient the acquired point cloud in 3D space, any two corresponding points p_1, $p_2 \in \mathbb{R}^3$ with $p_1 \in SP_1$, $p2 \in SP_2$, are related by a rigid transformation.

$$p_1 = Rp_2 + T \qquad (1)$$

where R is a 3×3 rotation matrix, and $T \in \mathbb{R}^3$ is the translation vector. The transformed point of p'_2 (i.e., $p'_2 = Rp_2 + T$), and its correspondence p_1 in SP_1, do not exactly coincide because of measurement errors. Then, the transformation parameters for R and T can be found by minimization of the sum of distance $\sum \left\| p_1 - p'_2 \right\|^2$ between p_1 and p'_2. Therefore, the

major task is to calculate rotation and translation parameters between the two point clouds SP_1 and SP_2.

If a good priori alignment is provided and the point clouds share a large overlapping region, existing registration methods, such as the Iterative Closest Point (ICP, (Besl and McKay, 1992)) or Chen and Medioni's method (Chen and Medioni, 1991), achieve a good performance. However, those methods fail if the initial alignment given is too far away from the true relative position and orientation. Therefore, methods to obtain a good initial alignment are of importance.

3. THE TEST TERRESTRIAL LASER SCANS

In this paper, the test scans have been acquired using a Riegl LMSZ360I scanner, which has a single shot measurement accuracy of 12mm, field of view of 360°×90°and a range of about 200 m. At 0.12° step width, a full scan takes approximately four minutes and results in a maximum of 3000×750 = 2.25 million scanned points. We selected an area called "Holzmarkt" in the historic district of Hannover, Germany, as an example for a densely built-up area (Brenner et al., 2008). In order to obtain reference values, manual alignment using artificial targets has been carried out, leading to errors generally in the range of a few millimeters. Table 1 shows the relative positions and orientations of the scans for those combinations that have been used for the alignment tests. One can verify that the scanner has been placed at approximate distances of 5m and with arbitrary orientation. Using the reference values, we also calculated the overlap between scans (as shown in Table 2).

Pair	ω (°)	ϕ (°)	κ (°)	X(m)	Y(m)	Z(m)
01-02	-1.088	-0.112	51.731	-5.50	0.96	0.02
01-03	0.551	0.419	57.447	-10.69	1.87	0.08
01-03a	-25.707	15.540	62.495	-10.64	1.96	0.05
01-04	1.984	0.481	119.261	-16.77	2.53	0.14
01-05	-0.692	0.678	-118.535	-21.05	4.24	0.16
01-05a	40.577	-19.397	-111.274	-21.12	4.11	0.09
01-06	-0.154	0.276	29.409	-24.71	2.74	0.29
...	...	...	...	...	...	...
02-03	1.432	-0.958	5.733	-2.50	4.64	0.08
03-04	0.824	-1.174	61.834	-2.72	5.47	0.01
04-05	1.482	2.238	122.148	3.58	2.90	-0.08
05-06	0.096	0.665	147.948	3.07	-2.51	0.07
...	...	...	...	...	...	...

Table 1: Reference values for the relative orientation of scan pairs. (First part: relative orientation of SP_1 and all other scans. Second part: relative orientation of successive scans. The tilted scans, which were marked with an "a" suffix, were acquired at the same positions as the upright scans.)

Pair	Overlap (%)	Pair	Overlap (%)
01-02	83.1	02-03	82.6
01-03	77.7	03-04	81.3
01-03a	73.3	04-05	83.6
01-04	68.8	05-06	80.3
01-05	63.0	...	...
01-05a	59.7		
01-06	50.5		

Table 2: Overlap percentage for the scan pairs used for the alignment tests. (First column: overlap of SP_1 with all other scans. Second column: overlap of successive scans.)

4. PROPOSED ALGORITHM

Nowadays, almost all the terrestrial laser scanners can return the distance from the point on surface and the energy of the backscattered laser light in this point for each measurement. This leads to two different sets of data. The 3D data are recorded from the distance measurement, whereas a panorama image can be generated from the reflectivity information. We will refer to this image as the reflectance intensity image for it looks similarly to a real intensity image taken by cameras.

4.1 Preprocessing of Reflectance Intensity Images

The reflectance intensity image is generated from the backscattered laser light which is a signal of high dynamic range. The strength of the return varies over a large range, from almost no return due to low reflective, far away surfaces, to direct reflection from retro reflective material. For the Riegl LMSZ360I this fact is accounted for by storing the reflectance information as 16-bit numbers. Since most of the displays and many standard image processing tools are still designed for 8-bit image data, we decide to convert the reflectance information to 8-bit. As shown in Figure 1, due to lost information in the course of conversion from 16-bit data, the 8-bit reflectance intensity image has characteristic of low contrast (as shown in Figure 1(a)). Therefore, we have to firstly apply image preprocessing to make this low contrast image appear more like a typical intensity image.

Histogram equalization and normalization are usual tools for increasing the contrast of images, especially when the usable data of the image is represented by close contrast values. Histogram equalization and normalization can be outlined as follows:

1. Histogram equalization accomplishes increasing the contrast of images by effectively spreading out the most frequent intensity values. A disadvantage of the method is that it is indiscriminate. It may increase the contrast of background noise, while decreasing the usable signal. Consider a reflectance intensity image, and let n_i be the number of occurrences of the gray level i. The probability of an occurrence of a pixel of level i in the image is

$$p(i) = n_i / n, \ i \in 0, \ldots, \ L-1 \qquad (2)$$

L being the total number of gray levels in the image, n being the total number of pixels in the image, and p being in fact the image's histogram, normalized to [0, 1]. Let us also define c as the cumulative distribution function corresponding to p, defined by:

$$c(i) = \sum_{j=0}^{i} p(x_i) \qquad (3)$$

where c also known as the image's accumulated normalized histogram. We would like to create a transformation of the form $y= T(x)$ that will produce a level y for each level x in the original image, such that the cumulative probability function of y will be linearized across the value range. The transformation is obtained by: $y_i = T(x_i) = c(i)$. Notice that the T maps the levels into the domain of [0, 1]. In order to map the values back into their original domain, the following simple transformation needs to be applied on the result:

$$y_i' = y_i (Max - Min) + Min \qquad (4)$$

2. Histogram normalization stretches an image's pixel values to cover the entire pixel value range (0 – 255). The intensity image is preprocessed by subtracting the minimum grey value from each pixel and dividing by its max–min range. Visually the image appears to have increased in contrast.

$$y_i' = ((y_i - Min)/(Max - Min)) \times 255.0 \qquad (5)$$

Böhm and Becker (Böhm and Becker, 2007) apply histogram equalization to increase the contrast of reflectance image. Then they extract the SIFT features and match these features in equalized reflectance image. However, in this paper, we prefer applying histogram normalization instead of equalization because the histogram normalization operator does not increase the contrast of background noise which usually leads to false matches. After this preprocessing, we take the advantage that we can rely on a standard implementation for feature extraction and do not have to alter lots of parameters.

4.2 SIFT Feature Based Key Points Matching

The Scale Invariant Feature Transform (SIFT) developed by Lowe (2003) is invariant to image scale and rotation, and provides robust matching across a substantial range of affine distortion, change in 3D viewpoint, addition of noise, and change in illumination. Our application employs a standard SIFT feature extraction and key point matching based on those features. For example, Figure 1(c) shows 301 matches obtained from 12093 extracted SIFT feature points.

4.3 Geometric Constraint

Due to invalid points, holes, dark or reflective spots on the object's surface, especially symmetry and self-similarity of the façade structures in the scans, the pairs of matched points contain a lot of false matches. As shown in Figure 1(c), repetitive elements such as windows and bricks on the ground, which are especially dominant in the example scene, cause false matches, when the geometry of the scene is ignored.


Original reflectance intensity image
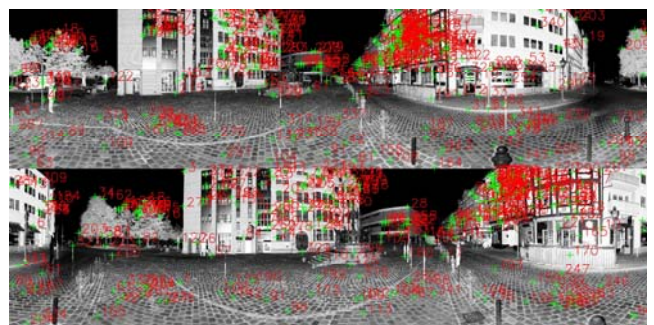
Matching result from equalized reflectance image
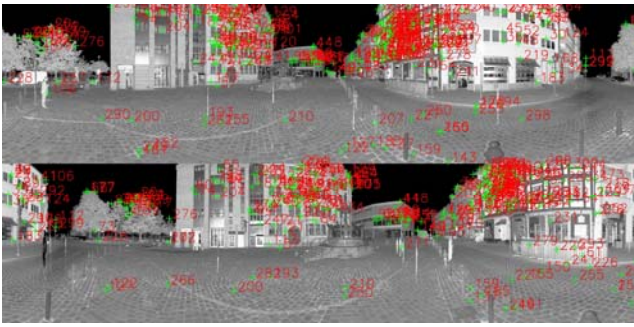
(c) Matching result from normalized reflectance image

Figure 1: Comparison of the matching result between SP$_1$ and SP$_2$ from histogram equalization and normalization using SIFT method.

In our method, we include the discrete geometric properties of the key points to exclude false matches from the registration. In particular, the Gaussian and mean curvature values are computed based on the method of Cohen-Steiner and Jean-Marie (Cohen-Steiner and Jean-Marie, 2003) because of its time-efficiency, accuracy, and generality. There are some open problems to address for computing geometric curvatures in scans: One is ensuring that the point is on an object and not part of the background. Another is that the objects in different depths have a different appearance in the range image. Objects that are closer to the scanner are described by more points and have a more dominant appearance compared to objects that are further away. Therefore, the scanner placement significantly influences the object representation in the data. This dependency leads in turn to a bias in the number of extracted feature-points, favoring closer objects, and causing same objects to be described by different curvature values. In addition, discrete curvature is second-order derivatives of the surface which is sensitive to noise and small perturbations.
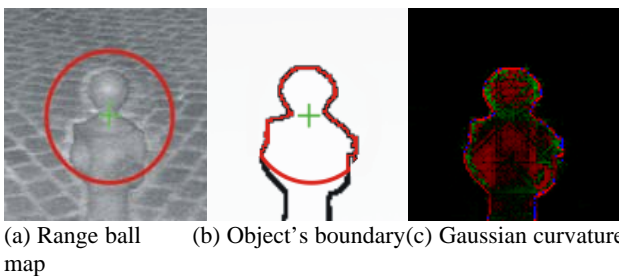
(a) Range ball   (b) Object's boundary(c) Gaussian curvature map

Figure 2: Curvature estimation within the bounding ball.

However, in the case of laser scanning point clouds, the scale, viewpoint and the relationship of neighbor points are known. Based on the above information, we use the Euclidean distance between neighbor points to distinguish the different objects in scenes avoiding erroneous calculation of curvatures. We propose an approach which estimates the curvature of a point and not only covers neighborhoods of variable size but also takes into account the topology of the surface in that neighborhood. As shown in Figure 2(a), our approach is based on a bounding ball whose center is at each point of the matches, whose radius represents the scale at which the shape is analyzed, and whose boundary intersects the object's boundary (as shown in Figure 2(b)). In our method, we set the radius as 0.5m. We calculate the discrete curvature of a center point and also taking

into account the Gaussian-weighted curvatures of its neighboring points within the radius. By doing that, most influence of the scanner placement and noise can be reduced.

As far as correct matches are concerned, the curvature values of the pair points should be close. Ideally, the difference of pair points' curvature values should be zero. However, for the reason that noise and errors do exist in scans, we can consider the pair points as correct matches when its curvature difference is relatively close to zero. Finding the standard deviation of curvature difference between two entire point clouds is unrealistic because they are not one-to-one correspondence between each other. In most cases, the standard deviation is estimated by examining a sample taken from the data set. The most common measure used is the Sample Standard Deviation (SSD). In our method, we set the threshold as 3σ, where σ is the SSD of the curvature difference of the candidate matches and can be calculated as follows:

$$\sigma_k = \sqrt{\frac{1}{n-1}\sum_i^n (K_1 - K_2)^2}$$

$$\sigma_H = \sqrt{\frac{1}{n-1}\sum_i^n (H_1 - H_2)^2} \qquad (6)$$

where K_1 and H_1, K_2 and H_2 are the Gaussian and mean curvatures of matches in SP$_1$ and SP$_2$, respectively and *n* is the number of candidate matches. Due to the lack of texture information in the reflection image, we find the matched points on planar surface, such as wall and ground, usually turn out to be false matches. Therefore, we take the points as false matches if their curvature values are less than a certain threshold. In our method, we calculate the Sample Standard Deviation of the Mean (SSDM) of Gaussian and mean curvatures as the threshold:

$$\tau_{K_1} = \sqrt{\frac{1}{n-1}\sum_i^n (K_1 - \bar{K})^2}$$

$$\tau_{K_2} = \sqrt{\frac{1}{n-1}\sum_i^n (K_2 - \bar{K})^2}$$

$$\tau_{H_1} = \sqrt{\frac{1}{n-1}\sum_i^n (H_1 - \bar{H})^2}$$

$$\tau_{H_2} = \sqrt{\frac{1}{n-1}\sum_i^n (H_2 - \bar{H})^2} \qquad (7)$$

To sum up, we regard the candidate matched points as correct matches if they meet following outlines, otherwise they should be excluded as false matches.

1. $K_1 > \tau_{K_1}$ AND $H_1 > \tau_{H_1}$;

2. $K_2 > \tau_{K_2}$ AND $H_2 > \tau_{H_2}$;

3. $\left| K_1 - K_2 \right| < 3\sigma_k$;

4. $\left| H_1 - H_2 \right| < 3\sigma_H$

Therefore, in our method, we can safely exclude the false matches according to the deviation of geometric curvature of the matches. The full scene of Gaussian and mean curvature map of SP$_1$ are shown in Figure 3, where red color is for

positive values, green for negative, and blue for invalid points (such as points in the sky).
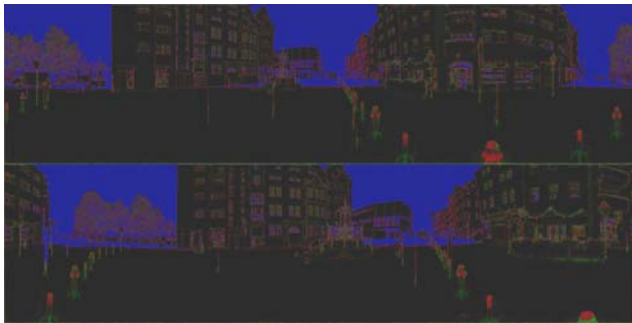
(a)   Gaussian curvature map
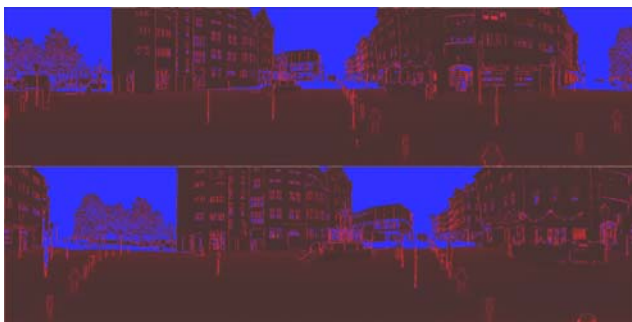
(b)   Mean curvature map

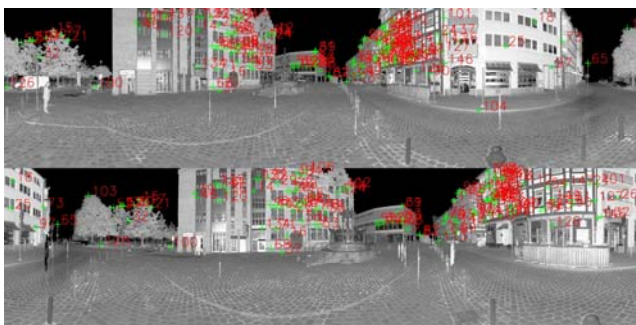Figure 3: Gaussian and mean curvature map of SP_1 and SP_2.

Figure 4: Matching result between SP_1 and SP_2 with geometric constraint.

Although the SIFT method with geometric constraint already provides good matching results, false matches are nevertheless possible because lots of structures, which are similar in both gray scale and geometric shape, do exist in test scene. Since the following registration steps are sensitive to such false correspondences, we apply an additional filtering to the matches based on the RANSAC method (Fischler and Bolles, 1981). Randomly a sample of point pairs is drawn from all SIFT matches. From the pair of three points a rigid body transformation is computed. All SIFT matches are checked against this transformation for consensus. The sample with the largest consensus is selected for registration. Figure 4 shows the 151 matches from 301 candidate pairs of points by using geometric constraint. Only 116 are confirmed as valid 3D corresponding tie points using RANSAC (as shown in Figure 5).

Since the rotation matrix R and translation vector T for initial alignment is available now, the ICP algorithm (Chen and Medioni, 1991) (Besl and McKay, 1992), which alternately establishes correspondences and refines the transformation parameters R and T, achieve a good performance and align two point cloud by minimizing the error metric derived from the distance between them.
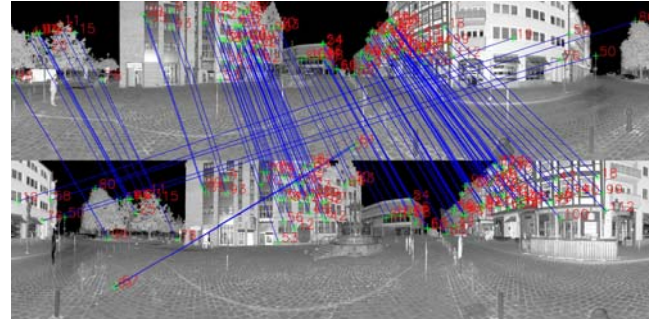

Figure 5: Best consensus matches found through RANSAC imported as tie points for registration.

5.   EXPERIMENTS

As described in Section 4, the first step is preprocessing of reflectance intensity image. Then the SIFT features are extracted and matched from both reflectance images. As an example, Figure 6(a) shows the total number of matches from equalized or normalized reflectance image between SP_1 and all other scans. However, Figure 6(b) shows the number of correct matches from equalized or normalized reflectance image. The correct matches are defined as the pairs of points whose distance ($\left\| p_1 - p_2' \right\|^2$) between p_1 and p_2' ($p_2' = Rp_2 + T$) is less than 0.5m. One can see the normalized images achieve better performance by involving more correct matches and less total matches.
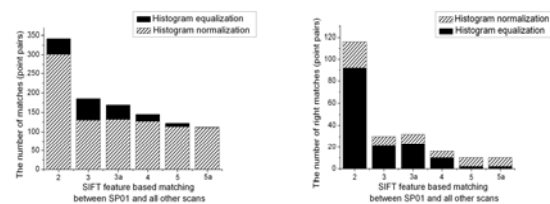
(a)The number of total matches (b)The number of correct matches

Figure 6: Numerical comparison of the matching results between SP_1 and all other scans from histogram equalization and normalization using SIFT method.

Figure 7(a) identifies the proposed geometric constraint improves the ratio of correct matches greatly. Figure 7(b) shows most correct matches are placed between 10m and 60m from the scanner and almost cover all around the scene. Therefore, we can expect accurate results by using these matches to calculate position and orientation parameters. Table 3 shows that by using geometric constraints we can safely exclude most of false matches and at the same time keep all the correct matches. The proposed method can improve the ratio of correct matches by a factor of more than two.
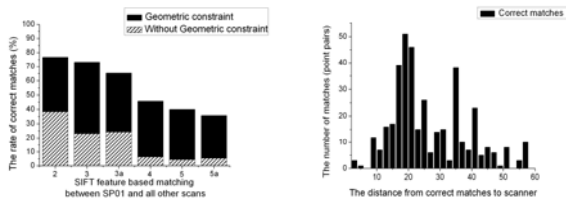
(a) Ratio of correct matches (b) Distance from points to scanner
Figure 7: Compare the matching results with and without geometric constraint.

The resulting position and orientation errors for our method are shown in Table 4. In order to evaluate the registration results, we compared the planar patch approach (Dold and Brenner, 2006) with our proposed method using the reference orientation. In (Brenner et al., 2008), the orientation by planar patches was able to align SP_1 with SP_{10} which have an overlap of 16%. In contrast, it seems that the proposed method is more influenced by scene contents. The proposed method fails after SP_{5a}, which has a considerably larger overlap of 50%. However, the distance between SP_1 and SP_{5a} is 20 m, which is probably anyhow meet the distance between two scans one would prefer to obtain a dense city scan with few occlusions.

Pair	Total matches	Right matches	Right ratio (%)	Total matches	Right matches	Right ratio (%)
01-02	301	116	38.5	151	116	76.8
01-03	130	30	23.1	45	30	73.2
01-03a	132	32	24.2	49	32	65.3
01-04	127	16	12.6	35	16	45.7
01-05	113	10	8.8	25	10	40.0
01-05a	111	10	9.0	28	10	35.7
01-06	107	2	1.9	21	2	9.5
02-03	437	172	39.4	216	172	79.6
03-03a	1714	1438	83.9	1597	1438	90.0
03-04	328	133	34.5	162	133	82.3
04-05	609	309	50.7	342	309	90.4
05-05a	1476	1220	82.7	1352	1220	90.2
05-06	235	194	82.6	209	194	92.8

Table 3: Comparison of matching results with or without geometric constraint.

Pair	$\triangle\omega\,(°)$	$\triangle\phi\,(°)$	$\triangle K\,(°)$	$\triangle X(m)$	$\triangle Y(m)$	$\triangle Z(m)$
01-02	-0.031	-0.001	0.022	-0.001	-0.017	0.010
01-03	0.051	-0.082	-0.078	0.018	0.021	0.038
01-03a	-0.075	-0.013	-0.032	0.032	-0.048	0.051
01-04	0.037	0.079	0.021	-0.053	-0.011	-0.025
01-05	-0.028	-0.104	0.115	-0.056	0.051	0.047
01-05a	-0.108	0.126	0.022	0.091	-0.039	0.013
01-06	—	—	—	—	—	—
02-03	-0.018	0.011	-0.009	-0.031	0.019	-0.017
03-03a	0.033	-0.009	-0.026	-0.027	-0.021	0.009
03-04	-0.031	0.018	-0.013	0.017	-0.018	0.007
04-05	0.042	-0.020	-0.016	-0.033	0.032	0.012
05-05a	-0.023	0.019	-0.021	-0.025	-0.016	-0.014
05-06	0.029	-0.014	-0.011	0.016	-0.022	0.019

Table 4: Deviation of the translation and rotation parameters from the reference values for the registration based on proposed method

On the other hand, the proposed registration method has the advantage of being algorithmically simple and does not rely on the presence of planar structures. In addition, the proposed method is conceptually simpler and faster. Therefore, if it is to be preferred depends strongly on the application. As far as accuracy of proposed method is concerned, one can see that the maximum deviation from the reference is less than 10cm in translation, and 0.2° in orientation. This is better than the planar patch method which achieved a maximum deviation of less than 20cm in translation, and 0.5° in rotation angles.

Considering the required computation time, SIFT feature based matching took an average of 20s. In the case of computing Gaussian and mean curvature, it is quite time consuming to generate the full scene of curvature map. In practice, we only compute the Gaussian and mean curvature in the neighborhood of matched points. This is very quick and takes around 5s. Then a standard RANSAC will take another 5s. Thus, in total, approximately 30s were required on average to match two scans on a 2GHz Pentium laptop.

6. CONCLUSIONS AND FUTURE WORK

We have shown a key point based automatic method using intensity and geometry features for the marker-free registration of terrestrial laser scans. The method uses SIFT feature based key points extracted from the normalized reflectance image with geometric constraint. Results and the analysis show the proposed method's efficiency and robustness. The method can be used to register laser scanning data at accuracy comparable to that of manual registration using natural tie points.

For the future work, several issues are worth investigating. Our approach applies the SIFT method to extract feature points. Furthermore, other feature points, such as corner points, can be detected as geometric primitives by using Harris or SUSAN operators. In addition to using a geometric constraint, other primitives can probably be used for the prioritization of the correspondences. And finally, the proposed algorithm offers a pair-wise registration scheme. It can be extended into a multi-scan registration.

REFERENCES

Bae, K. and Lichti, D., 2004. Automated registration of unorganised point clouds from terrestrial laser scanners. International Archives of Photogrammetry and Remote Sensing 35 (Part B5), pp. 222–227.

Barnea, S. and Filin, S., 2008. Keypoint based autonomous registration of terrestrial laser point-clouds. ISPRS Journal of Photogrammetry & Remote Sensing, Theme Issue: Terrestrial Laser Scanning 63, pp. 19–35.

Bendels, G. H., Degener, P., Wahl, R., Körtgen, M. and Klein, R., 2004. Image-based registration of 3d-range data using

feature surface elements. In: The 5th International Symposium on Virtual Reality, Archaeology and Cultural Heritage.

Besl, P. J. and McKay, N. D., 1992. A method for registration of 3-d shapes. IEEE Transactions on Pattern Analysis and Machine Intelligence 14(2), pp. 239–256.

Böhm, J. and Becker, S., 2007. Automatic marker-free registration of terrestrial laser scans using reflectance features. In: 8th Conf. on Optical 3-D Measurement Techniques, Zurich, pp. 338– 344.

Brenner, C., Dold, C. and Ripperda, N., 2008. Coarse orientation of terrestrial laser scans in urban environments. ISPRS Journal of Photogrammetry & Remote Sensing, Theme Issue: Terrestrial Laser Scanning 63, pp. 4–18.

Chen, Y. and Medioni, G., 1991. Object modeling by registration of multiple range images. In: International Conference on Robotics and Automation, Vol. 3, pp. 2724–2729.

Cohen-Steiner, D. and Jean-Marie, M., 2003. Restricted delaunay triangulations and normal cycle. In: the 19th Conference on Computational Geometry, Vol. 53, San Diego, California, pp. 312–321.

Dold, C. and Brenner, C., 2006. Registration of terrestrial laser scanning data using planar patches and image data. International Archives of the Photogrammetry, Remote Sensing and Spatial Information Sciences 36 (Part 5), pp. 25–27.

Fischler, M. A. and Bolles, R. C., 1981. Random sample consensus: A paradigm for model fitting with applications to image analysis and automated cartography. Communications of the ACM 24(6), pp. 381–393.

Lowe, D., 2003. Distinctive image features from scale-invariant keypoints. In: International Journal of Computer Vision, Vol. 20, pp. 91–110.

Rusinkiewicz, S. and Levoy, M., 2001. Efficient variants of the icp algorithm. In: Third Int. Conf. on 3D Digital Imaging and Modeling (3DIM), Quebec, Canada, pp. 142–152.